

The clinical guiding value of a radiomics model for androgen deprivation therapy for prostate cancer

Journal of International Medical Research
49(6) 1–13

© The Author(s) 2021

Article reuse guidelines:

sagepub.com/journals-permissions

DOI: 10.1177/03000605211014301

journals.sagepub.com/home/imr



Na Yu¹ , Baoping Wang¹, Jialiang Ren²,
Hui Wu³ , Yang Gao³, Aishi Liu³ and
Guangming Niu³

Abstract

Objective: Three models were used to evaluate prostate cancer after androgen deprivation therapy (ADT) and to determine the value of detecting residual lesions after treatment.

Methods: We retrospectively analysed patients with prostate cancer who received ADT from January 2018 to June 2019. Patients were divided into ADT responder and ADT non-responder groups, and clinical risk factors were determined. Regions of interest were manually contoured on each slice on fat-saturated-T2-weighted imaging, and radiomic features were extracted. Uni- and multivariate logistic regression were used to establish radiomics, clinical and combined models.

Results: There were 23 ADT non-responders and 20 ADT responders. In the clinical model, total prostate-specific antigen concentration and T stage were independent predictors of efficacy (area under the curve (AUC) = 0.774). The characteristics, MinIntensity and Correlation_angle135_offset4 indicated an effective clinical model (AUC = 0.807). GLCMEntropy_AllDirection_offset1_SD was the best feature to differentiate residual lesions from the central gland (CG) (Lesion-CG model, AUC = 0.955). Correlation_angle135_offset4, GLCMEntropy_AllDirection_offset4_SD and GLCMEntropy_AllDirection_offset7_SD differentiated residual lesions from the peripheral zone (PZ) (Lesion-PZ model, AUC = 0.855). The AUC for the combined model was 0.904.

¹Department of Imaging Diagnosis, The Fifth People's Hospital of Datong, Datong, Shanxi Province, China

²General Electric Pharmaceutical (Shanghai), Beijing, China

³Department of Imaging Diagnosis, Affiliated Hospital of Inner Mongolia Medical University, Hohhot, Inner Mongolia, China

Corresponding author:

Guangming Niu, Department of Imaging Diagnosis, Affiliated Hospital of Inner Mongolia Medical University, No. 1, Channel North Street, Huimin District, Hohhot, Inner Mongolia 10050, China.
Email: Cjr.niuguangming@vip.163.com



Conclusions: Our models can guide the clinical treatment of patients with different ADT responses. Furthermore, the radiomics model can detect prostate cancer that is non-responsive to ADT.

Keywords

Radiomics, prostate cancer, androgen deprivation treatment, magnetic resonance imaging, clinical model, logistic regression analysis

Date received: 1 October 2020; accepted: 29 March 2021

Introduction

Prostate cancer is the second most common malignancy in men after lung cancer,¹ with large individual differences and a long natural course. Androgen deprivation therapy (ADT) is an effective treatment for advanced prostate cancer.² However, although chemical castration can slow the progression of prostate cancer, relieve symptoms and prolong life, some patients are non-responsive to ADT and will have residual lesions after treatment. Clinically, the prostate-specific antigen (PSA) concentration and Gleason score are commonly used to evaluate the efficacy of ADT,^{3,4} but these fail to provide guidance for the next treatment. Multi-parameter magnetic resonance imaging (Mp-MRI) has high sensitivity in detecting and locating prostate cancer lesions.⁵ However, ADT causes significant changes in prostate appearance and signals on MRI, which may overestimate or misdiagnose residual tumours.⁶ Therefore, a more accurate and suitable method is needed to monitor the progression of prostate cancer after ADT, and intensive treatment for more invasive lesions is helpful in disease management.

Radiomics is a new technology that uses mathematical methods to evaluate the grey-scale intensity and pixel position in an image. This method can be used to extract quantitative data from standard medical images and can help improve clinical

diagnosis and decision making.⁷ Recently, radiomics has been used in patients with prostate cancer to differentiate between prostate cancer and benign hyperplasia,⁸ monitor risk stratification⁹ and predict biochemical recurrence.^{10,11} However, radiomics has not been commonly used to detect and describe prostate cancer in patients after undergoing ADT. Therefore, our hypothesis was that the extracted radiomics features from MR images can reflect the tissue pathological changes after ADT and that the features can be used to guide clinical treatment (adding antiandrogen intensive therapy or intensifying focal therapy).¹²

In this study, first, we evaluated the value of a clinical model, radiomics model and combined model after ADT in the ADT non-responder group to provide clinical guidance and to differentiate residual lesions from the peripheral zone (PZ) and central gland (CG) to lay the foundation for focal therapy. Second, we attempted to verify whether a combined model is more helpful to determine the next treatment.

Methods and Materials

Patients

Patients who met the inclusion criteria from January 2018 to June 2019 were retrospectively analysed. The study was approved by the ethics committee of our hospital, and

written informed consent was obtained from all subjects. The inclusion criteria were as follows: (1) Patients were confirmed to have clinical \geq stage 2 prostate cancer before ADT. (2) Patients received ADT for 7 months, and all patients were receiving the last ADT at the time of imaging. (3) The inclusion criteria for the ADT non-responder group were that the PSA concentration was still increased after 7 months of treatment (of three consecutive PSA tests performed once a week, if two test results were equivalent to a 50% increase in the lowest value or one test revealed PSA $>$ 2 ng/dL). Mp-MRI was used to biopsy the suspected residual lesions, and the detailed pathological results (12-point transrectal ultrasound-guided puncture including the insertion angle and depth) were combined with Mp-MRI to locate the residual lesions. (4) The inclusion criteria for the group with good efficacy were PSA concentrations within the normal range, no Mp-MRI suspicious lesions and negative pathological results after treatment. (5) The serum testosterone concentrations of the patients reached castration level after treatment ($<$ 1 nmol/L). (6) All enrolled

patients had complete imaging data (MRI, positron emission tomography-computed tomography (PET-CT)). The exclusion criteria were as follows: (1) patients with poor image quality that did not meet the requirements; (2) patients who received other treatments, such as radiation or surgery and (3) patients with the largest diameter of the residual lesions in the identified model $<$ 1.0 cm and a total tumour area volume of interest (VOI) that could not be accurately delineated. The inclusion and grouping of cases are shown in Figure 1. Androgen deprivation was achieved with androgen receptor antagonists for treatment, namely bicalutamide (orally, 50 mg once a day) or cyproterone acetate (orally, 100 mg three times a day) for 7 consecutive days followed by subcutaneous injection of 10.8 mg of luteinising hormone-releasing analogue (LHRHA), which is known to achieve castration within 14 days, as determined by serum testosterone concentrations.¹³

MRI acquisition

We used an American GE 3.0-T Discovery 750 MR scanner (General Electric

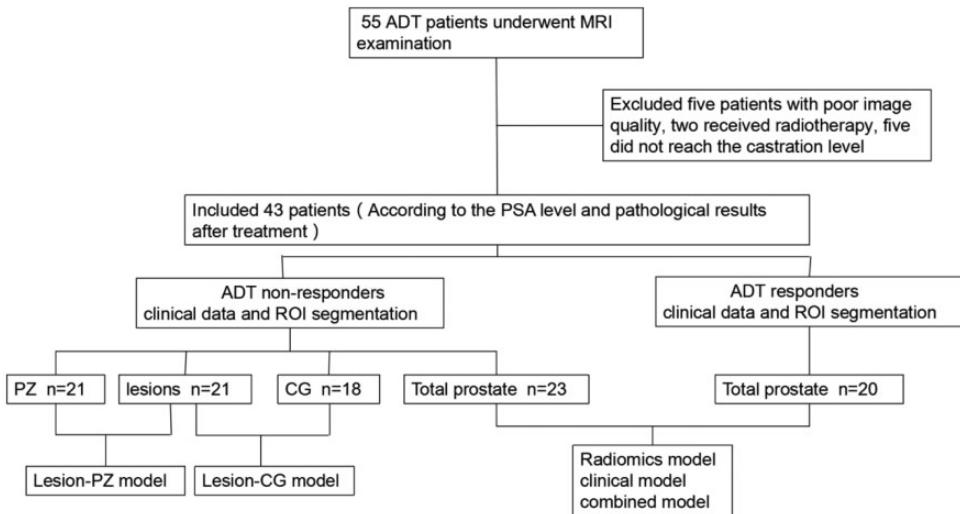


Figure 1. Patient allocation.

Healthcare, Milwaukee, WI, USA) with an eight-channel phased array coil as the receiving coil. Before the scan, the patient had a moderately full bladder and was placed in the supine position. The scan centre was located 2 cm above the pubic symphysis. Scanning sequences constituted axial, sagittal and coronal T2-weighted images (T2WI), axial T1-weighted images (T1WI) and diffusion-weighted image (DWI) sequences. The main imaging sequences were axial (AX) fat-suppressed (FS) T2WI and DWI, AX FS T2WI spin-echo sequences (repetition time/echo time (TR/TE), 3522/85; slice thickness, 4.0 mm; slice gap, 1 mm; number of excitations (NEX), 4; matrix, 320×192 and field of view (FOV), 240×240 mm). DWI acquisition constituted a single-shot echo-planar imaging sequence (TR/TE, 3600/64.1; slice thickness, 4.0 mm; slice gap, 1 mm; NEX, 8;

matrix, 128×128 ; FOV, 300×300 mm; b value, 0 s/mm^2 and 1500 s/mm^2).

Radiomics model

All patients' MRI images were exported and stored in digital imaging and communications in medicine (DICOM) format on a picture archiving and communication system (PACS) workstation. The process was as follows: image standardisation, manual image segmentation, feature extraction and feature selection, model building and model performance, as shown in Figure 2. On FS-T2WI (T2WI residual lesions could be visualised more clearly after fat suppression) images, two experienced pelvic MRI radiologists performed the delineation and synthesis of a three-dimensional (3D) VOI using itK-Snap (version 3.6.0, www.itksnap.org) software. The sketching criteria were as follows: (1)

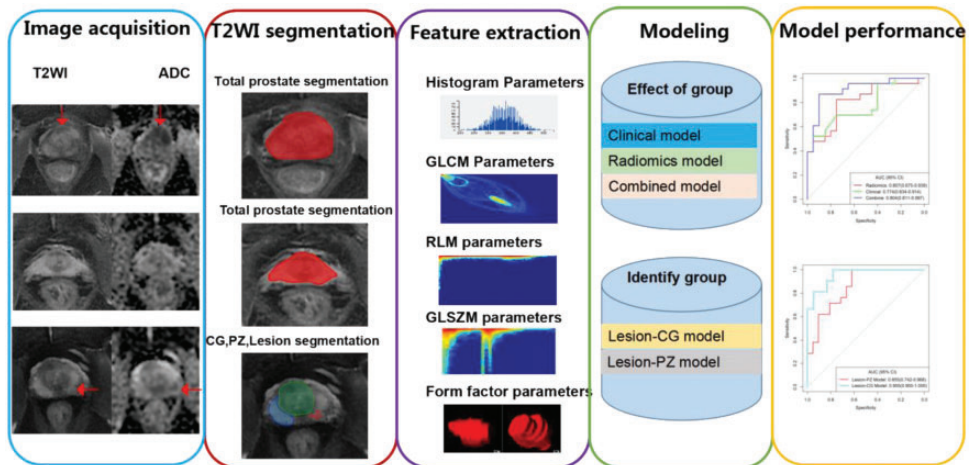


Figure 2. Workflow of the radiomics analysis. Prostate fat-saturated T2-weighted imaging (FS-T2WI) was used to extract the features, and apparent diffusion coefficient (ADC) imaging was used as the reference. In the image segmentation, from top to bottom, the total prostatic volume was segmented in the ADT non-responders, and the lesions were located in the central gland (CG) of the prostate (red arrow). Regarding total prostate volume segmentation in the ADT responders, the lesions were divided by volume (red area), peripheral zone (PZ) (blue area) and central gland (CG) (green area). An example of feature extraction shows the features covered by T2WI radiomics and a modelling example in the effect groups (clinical model, radiomics model and combined model) and identification groups (Lesion-CG, Lesion-PZ). Finally, the model was evaluated.

The total prostate volume of the two groups was delineated inward at 3 mm, excluding the interference of surrounding soft tissue. (2) PZ delineation criteria for the ADT non-responders: The delineated areas were pathologically confirmed to be free of residual lesions, with 8 cases of the unilateral left lobe outlined, 10 cases of the unilateral right lobe outlined, and 3 cases of bilateral lobes outlined. (3) CG delineation criteria of the ADT non-responders: Except for 3 patients whose lesions were pathologically confirmed to be located in the central gland, the remaining 18 patients underwent full central gland delineation with the edge turning inward by 3 mm. (4) Criteria for delineation of residual lesions: For suspected lesions examined by Mp-MRI, rectal ultrasound-guided biopsy was performed for region of interest (ROI) localisation of residual lesions. Three cases were located in the CG, and 18 cases were located in the unilateral PZ (left or right lobe). The apparent diffusion coefficient (ADC) images were then compared.

Radiomics software that uses Artificial Intelligence Kit (AK) (GE healthcare) software was applied to extract all quantitative radiomics features from VOIs labelled on T2WI, with 396 radiomics features (histogram features, grey level co-occurrence matrix (GLCM), run-length matrix (RLM), grey-level size zone matrix (GLSZM) and form factors. Feature extraction and radiomics analyses were performed as follows: 1. For data preprocessing, the outliers were replaced by the median, and the data were standardised by z-scores to unify the scales of all characteristics. 2. Dimension reduction of feature numbers and univariate logistic regression were used to screen out features with $P < 0.05$. 3. Multivariate logistic regression was used to model the selected features, and the Akaike information criterion (AIC) was used as the stopping principle to select the optimal feature subset, step by step. Finally, the remaining features were used

to identify and establish three logistic regression models, namely one effect model (radiomics model) and two identification models (Lesion-CG model and Lesion-PZ model), as shown in Figure 2.

Clinical and combined model

Age, family history, symptoms (asymptomatic and symptomatic frequency of urination, urinary pain, lumbosacral pain, sexual dysfunction and bone pain), PSA concentration, Gleason grade, T stage, lymph node metastasis and distant metastasis before treatment were included in the clinical data. All patients underwent transrectal ultrasound-guided needle prostatic biopsy before and after ADT. All patients also underwent PET-CT imaging to identify regional lymph node metastasis and distant metastasis. After univariate logistic regression analysis of the clinical data, multivariate logistic regression was used to identify the feature combinations with the highest diagnostic efficacy for indicators with statistically significant differences. Logistic regression analysis was also used to establish a combined model by combining the selected radiomics and clinical characteristics.

Clinical application value

Nomogram analysis was used to assess the potential clinical application of the best model. A calibration curve was drawn to assess the degree of deviation between the predicted results of the test and the actual results. The deviation between the calibration curve and a 45° line in each model reflected the prediction performance of each model. To determine the clinical practicability of each model to evaluate the therapeutic efficacy of ADT, decision curve analysis (DCA) was applied. We developed three decision curves: a clinical model, a radiomics model and a combined model. The clinical usefulness of each model was

evaluated by calculating the net benefits of a series of threshold probabilities.

Histopathological analysis

Two pathologists with, respectively, 10- and 20 years' experience in urology examined the specimens separately. According to the Gleason grading system, tumours are graded according to the type of tissue structure (grade 1–5), and the final score was obtained by selecting the two most important component grades.¹⁴ The two pathologists scored each tissue sample from 12 puncture specimens and provided a total score, which was the reference standard for our model.

Statistical analysis

Using R software (version 3.6.1 track, www.r-project.org) to analyse the data, the intraclass correlation coefficient (ICC) was used to evaluate the consistency of the two radiologists in extracting the radiomics characteristics, and an ICC >0.80 indicated good consistency.^{15,16} The Kolmogorov–Smirnov test was used to evaluate whether the included features conformed to a normal distribution, and Levene's test was used to test the variance homogeneity. Clinical characteristics with a normal distribution and homogeneous variances (age, TPSA) were compared by two independent samples t-tests. The Chi-square test was used for numerical data (family history, symptoms, Gleason grade, T stage, lymph node metastasis and distant metastasis). After univariate analysis, multivariate logistic regression was used to select the most effective feature combination to establish the clinical model. We performed 200 bootstrap resamples for model repeatability evaluation. Receiver operating characteristic (ROC) curves and calibration curves were used to evaluate the diagnostic performance of the clinical, radiomics and

combined models. DCA was used to calculate the net benefit of the model under different clinical thresholds. All tests were two-sided, and $P < 0.05$ was considered significant.

Results

Patients

There were 23 ADT non-responders (mean age: 69.4 ± 8.56 years) and 20 ADT responders (mean age, 68.87 ± 7.19 years). After treatment, all patients were grouped according to the puncture pathology. Patients who still had lesions after treatment constituted the ADT non-responders group, while those without lesions after treatment constituted the ADT responders group.

Clinical model

The results of univariate and multivariate logistic regression analyses are shown in Table 1 and Table 2. The Gleason grade, TPSA, T stage and lymph node metastasis before treatment differed significantly between the two groups (all $P < 0.05$). There were no significant differences in age, symptoms, family history or distant metastasis. After backward stepwise multivariate logistic regression analysis, TPSA (odds ratio (OR): 1.036, 95% confidence interval (CI): 1.008–1.069; $P < 0.05$) and T stage (OR: 4.710, 95% CI: 1.212–21.532; $P < 0.05$) were independent predictive variables of efficacy. We then established the clinical model based on the independent variables, which had an area under the curve (AUC) of 0.774 (95% CI: 0.634–0.914), as shown in Table 3 and Figure 3a.

Radiomics model

Features with an ICC > 0.80 were retained, and 59 texture features with an ICC ≤ 0.8 were deleted from the radiomics model; 36

Table 1. Patients' clinical data.

Feature	Good effect (n = 23)	Poor effect (n = 20)	P
Age (Mean ± SD, years)	68.87 ± 7.19	69.4 ± 8.56	0.826
Symptoms (%)			0.853
Present	12 (52.2%)	11 (55%)	
Absent	11 (47.8%)	9 (45%)	
Family history (%)			0.158
Present	13 (56.5%)	7 (35%)	
Absent	10 (43.5%)	13 (65%)	
Distant metastasis(%)			0.298
Present	14 (60.9%)	9 (45%)	
Absent	9 (39.1%)	11 (55%)	
Gleason score (%)			0.023
≥7	16 (69.6%)	7 (35%)	
<7	7 (30.4%)	13 (65%)	
Lymph node metastasis (%)			0.043
Yes	14 (60.9%)	6 (30%)	
No	9 (39.1%)	14 (70%)	
TPSA (Mean ± SD, ng/m)	80.96 ± 24.61	61.25 ± 23.30	0.01
T stage(%)			0.023
T2	7 (30.4%)	13 (65%)	
T3	16 (69.6%)	7 (35%)	

SD, standard deviation; TPSA, total prostate-specific antigen; T stage, tumour stage.

Table 2. Multivariate logistic regression analysis results.

Variable	Clinical model OR (95% CI)	P	Combined model OR (95% CI)	P
TPSA	1.036 (1.008–1.069)	0.01	1.023 (0.988–1.064)	0.20
T stage	4.710 (1.212–21.532)	0.03	16.423 (2.497–225.938)	0.01

OR, odds ratio; CI, confidence interval; TPSA, total prostate-specific antigen; T stage, tumour stage.

texture features with an ICC \leq 0.8 were removed from the Lesion-CG model, and 54 texture features with an ICC \leq 0.8 were removed from the Lesion-PZ model. The remaining two characteristics in the uni- and multivariate logistic regression radiomics models were used to establish the efficacy evaluation model, namely, MinIntensity and Correlation_angle135_offset4 (AUC = 0.807; 95% CI: 0.675–0.939). The Lesion-PZ model included the three remaining features of Correlation_angle135_offset4, GLCMEntropy_AllDirection_offset4_SD and GLCMEntropy_

AllDirection_offset7_SD (AUC = 0.855; 95% CI: 0.742–0.968). The Lesion-CG model characteristics included the remaining feature, GLCMEntropy_AllDirection_offset1_SD, after selection (AUC = 0.955; 95% CI: 0.900–1.000), as shown in Table 3 and Figure 3a, 3b.

Combined model

The clinical and radiomics model features were regressed step by step to find the minimum AIC value to establish the combined model. Among the features, T stage

Table 3. Predictive performance of the different models.

	AUC (95% CI)	ACC (95% CI)	SEN (95% CI)	SPE (95% CI)	PPV (95% CI)	NPV (95% CI)
Clinical model	0.774 (0.634–0.914)	0.721 (0.563–0.847)	0.522 (0.261–0.739)	0.950 (0.599–1.000)	0.923 (0.857–0.944)	0.633 (0.521–0.645)
Radiomics model	0.807 (0.675–0.939)	0.791 (0.640–0.900)	0.826 (0.391–0.957)	0.750 (0.350–0.900)	0.792 (0.643–0.815)	0.789 (0.636–0.818)
Combined model	0.904 (0.811–0.997)	0.884 (0.749–0.961)	0.870 (0.348–1.000)	0.900 (0.500–1.000)	0.909 (0.800–0.920)	0.857 (0.769–0.870)
Lesion-CG model	0.955 (0.900–1.000)	0.897 (0.758–0.971)	1.000 (0.667–1.000)	0.778 (0.556–0.944)	0.840 (0.778–0.840)	1.000 (1.000–1.000)
Lesion-PZ model	0.855 (0.742–0.968)	0.810 (0.659–0.914)	1.000 (0.619–1.000)	0.619 (0.427–0.810)	0.724 (0.619–0.724)	1.000 (1.000–1.000)

AUC, area under the curve; CI, confidence interval; ACC, accuracy; SEN, sensitivity; SPE, specificity; PPV, positive predictive value; NPV, negative predictive value; CG, central gland; PZ, peripheral zone.

(OR: 16.423, 95% CI: 2.497–225.938; $P=0.011$), TPSA (OR: 1.023, 95% CI: 0.988–1.064) and radiomics indications (OR: 758.612, 95% CI: 14.536–201,509.930; $P=0.004$) were the final diagnostic factors to evaluate the efficacy of ADT. Although TPSA had a non-significant p-value, it was better to add TPSA without considering the P value when the stepwise regression was stopped with the AIC. The ROC analysis confirmed that the combined model was more effective than the clinical model or the radiomics model, with an AUC of 90.4% (95% CI: 0.811–0.997), accuracy of 88.4%, sensitivity of 87.0% and specificity of 90.0% (Table 3 and Figure 3a).

Predictive model evaluation. The AUC, accuracy, sensitivity, specificity, positive predictive value and negative predictive value of the five models are listed in Table 3. The ROC curve model comparing the three efficacy models and the two identification models is shown in Figure 3a, 3b. The bootstrap method showed that the combined model and Lesion-CG model had high AUC, sensitivity and specificity (Figure 3c).

When the clinical model, radiomics model and combined model were used to assess the efficacy of ADT, in the radiomics score waterfall plots (Figure 4), a score >0 represented predicted survival or lesion recurrence after ADT, and a score <0 represented good efficacy of ADT and no residual or recurrent lesions. Compared with the clinical model (Figure 4a) and the radiomics model (Figure 4b), the combined model (Figure 4c) significantly improved the false-negative and false-positive rates.

We chose a nomogram as a graphical representation of the combined model (Figure 5a). For example, a patient with 144 points would have a radiomics score of 0.91 (91 points), a pretreatment TPSA of 50 ng/m: (11 points), pretreatment tumour stage of T3 (42 points) and a 97% risk of poor

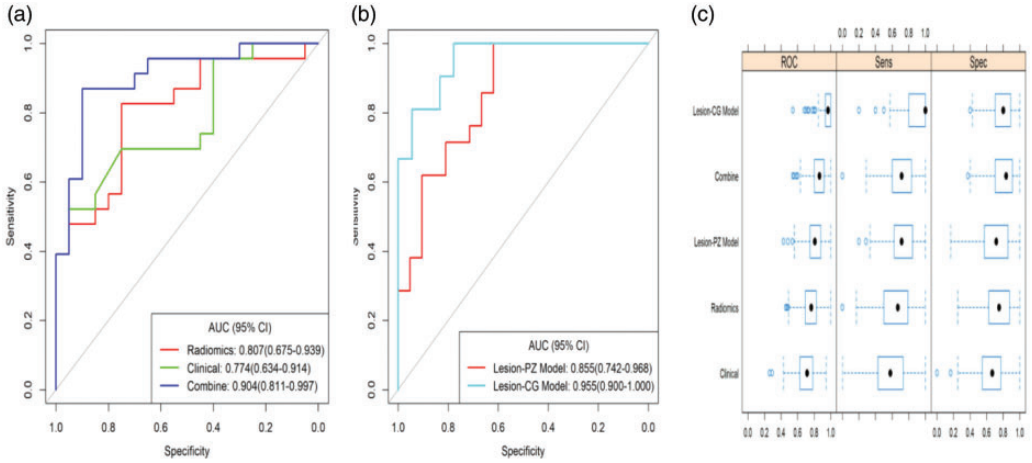


Figure 3. Receiver operating characteristic curves for the five models. (a) Receiver operating characteristic (ROC) curves for the radiomics model, clinical model and combined model. (b) ROC curves of the Lesion-peripheral zone (PZ) model and Lesion-central gland (CG) model. (c) A resampling method was adopted for the five models, and the distribution of the area under the curve (AUC), sensitivity and specificity of each model are shown on the horizontal axes.

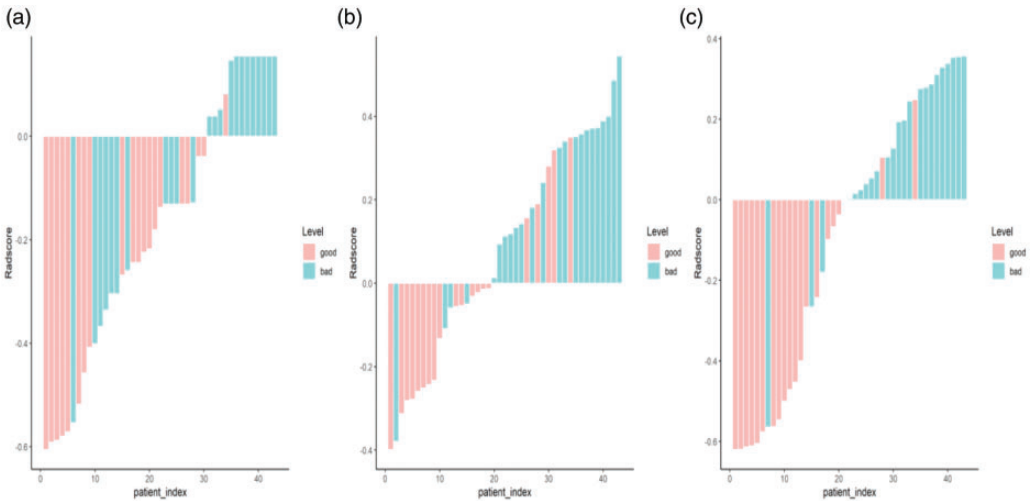


Figure 4. Radiomics score waterfall plots. Clinical model (a), radiomics model (b), and combined model (c).

effect after ADT. After DCA, the clinical, radiomics and combined models (Figure 5b) had net benefits under different risk thresholds. When the risk threshold value was 10% to 99%, the combined model for evaluating the clinical effect of ADT was

better than that of the clinical or radiomics model alone. Additionally, the net benefit of the three models was greater than the net benefit of all interventions and no intervention. The calibration curve in Figure 5c shows that the clinical model had a small

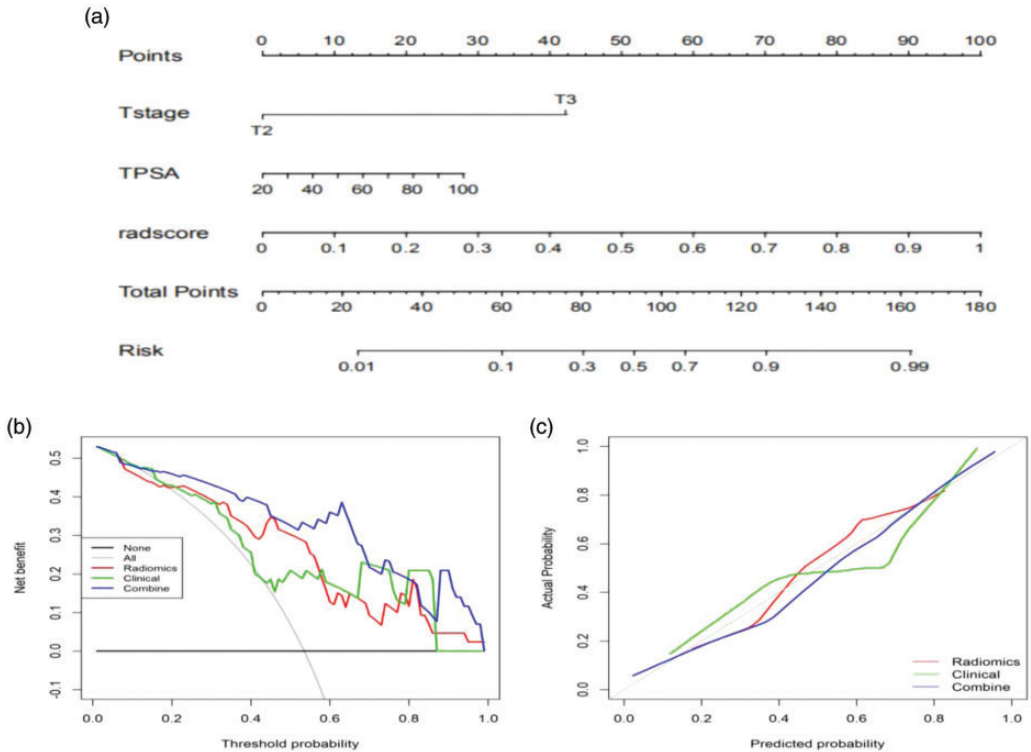


Figure 5. Development of a combined model nomogram (a) and decision curve analysis for the clinical, radiomics and combined models (b) and calibration curves of the clinical, radiomics and combined models. In (b), the decision curves for the three models to evaluate the efficacy of androgen deprivation therapy (ADT) are shown. In (c), the calibration curve describes the consistency of model prediction probability and observation probability. The 45° grey line represents the ideal prediction performance, while the solid coloured lines represent the diagnostic prediction performance of each model.

fluctuation in the evaluation of ADT efficacy, while the combined model showed good stability compared with the other models; the Hosmer–Lemeshow (HL) test demonstrated a non-significant value.

Discussion

In this study, we developed three models to monitor the efficacy of ADT and two identification models to differentiate residual lesions from peripheral benign tissue after ADT. Regarding monitoring ADT responses, the combined model constructed by combining the radiomics score with clinical factors showed better performance with DCA and

had a better AUC than the clinical model. This indicated that adding the radiographic radiomics score improved the diagnostic efficiency of the clinical factors. The radiographic nomogram successfully stratified patients with prostate cancer according to their risk of different treatment responses, which may contribute to individualised treatment decisions. The two identification models had higher accuracy and sensitivity for distinguishing between cancer foci and the surrounding tissues after ADT, which could improve the detection of residual cancer foci after ADT and guide further treatment.

Individualised treatment responses to ADT can be achieved by close monitoring

of serum PSA and testosterone concentrations, and with MRI. With close monitoring, clinical guidance can be provided at an early stage (with the addition of antiandrogens for intensive or focal therapy), to achieve the maximum benefit.¹⁷ Groenendaal et al.¹⁸ studied the effect of ADT on prostate cancer MR images as early as 2012 and found that ADT resulted in significant tumour reduction, impaired the detection of prostate cancer and limited the MRI guidance in clinical treatment. Therefore, we must improve the monitoring of ADT efficacy using different methods. The clinical, radiomics and combined models that we established can be used to monitor different therapeutic effects to guide the next clinical treatment. Although there were three false-negative cases and two false-positive cases in the radiomics score waterfall figure for the combined model, the cases' common characteristic was that the lesions could not be recognised owing to decreased T2WI signals caused by peripheral acinar atrophy after treatment.

ADT leads to atrophy of prostatic acinar cells, fibrosis and basal cell proliferation, thereby reducing the total glandular stroma and leading to a recognised decrease in total glandular volume. At the same time, T2 signals in the normal peripheral region are decreased, which affects the differentiation of tumour edges and limited diffusion in DWI, resulting in an increase in the overall prostatic signal.¹⁹ Currently, prostate cancer after ADT determined by conventional MRI is not ideal, and radiomics features can provide abundant quantitative characteristics that have good application prospects in the differentiation of tumours and benign tissues. In this study, the Lesion-CG model and the Lesion-PZ model differentiated tumour tissue from benign tissue with a diagnostic efficacy was 0.855 and 0.955, respectively.

Daniel et al.²⁰ studied the differentiation of tumour tissues from benign tissues using MRI texture analysis after ADT and found that texture characteristics differed between tumours and surrounding healthy tissues, consistent with the results of this study.

Limitations

This study had the following limitations: (1) The study design was retrospective, which may have led to selection bias. Ideally, the study design should be prospective, with MRI performed before and after ADT. (2) Owing to the limited sample size, it was impossible to build a verification set to verify the model. However, we used uni- and multivariate logistic regression analysis to select the parameters, which ensures the authenticity of the model, to a certain extent. (3) The total number of patients in our study was small ($n = 43$). In future research, we will link radiomics features with prostate histopathology by increasing the data volume. (4) We used only T2WI to extract the features because this modality provides high-resolution images for accurate ROI delineation, which directly affects the results. However, owing to the low signal-to-noise ratio and insufficient DWI resolution, this approach could not be used as an analysis model because the process of delineating lesions has an important impact on the analysis, which must be addressed carefully.^{21,22}

Conclusions

In this study, we found that MRI radiomics can be used to monitor ADT responses and to distinguish benign and tumour tissues after ADT. The results are of great value for determining the next step in prostate cancer diagnosis and treatment after ADT.

Declaration of conflicting interest

The authors declare that there is no conflict of interest.



Funding

This research received no specific grant from any funding agency in the public, commercial, or not-for-profit sectors.

Author contributions

All authors participated in the conception and design of the article and in drafting the manuscript, substantively revised the important content of the manuscript and approved the publication of the manuscript. All authors bear joint responsibility for the relevant parts of the manuscript's content.

ORCID iDs

Na Yu  <https://orcid.org/0000-0002-8716-6454>
Hui Wu  <https://orcid.org/0000-0002-1620-5321>

References

1. Rawla P. Epidemiology of prostate cancer. *World J Oncol* 2019; 10: 63–89.
2. Gillessen S, Attard G, Beer TM, et al. Management of patients with advanced prostate cancer: report of the Advanced Prostate Cancer Consensus Conference, 2019. *Eur Urol* 2020; 77: 508–547.
3. Valero J, Peleteiro P, Henríquez I, et al. Age, Gleason score, and PSA are important prognostic factors for survival in metastatic castration-resistant prostate cancer. Results of the Uroncor Group (Uro-Oncological Tumors) of the Spanish Society of Radiation Oncology (SEOR). *Clin Transl Oncol* 2020; 22: 1378–1389.
4. Narita S, Hatakeyama S, Takahashi M, et al. Clinical outcomes and prognostic factors in patients with newly diagnosed metastatic prostate cancer initially treated with androgen deprivation therapy: a retrospective multicenter study in Japan. *Int J Clin Oncol* 2020; 25: 912–920.
5. Weinreb JC, Barentsz JO, Choyke PL, et al. PI-RADS prostate imaging - reporting and data system: 2015, version 2. *Eur Urol* 2016; 69: 16–40.
6. Hötter AM, Mazaheri Y, Zheng J, et al. Prostate cancer: assessing the effects of androgen-deprivation therapy using quantitative diffusion-weighted and dynamic contrast-enhanced MRI. *Eur Radiol* 2015; 25: 2665–2672.
7. Summers RM. Texture analysis in radiology: Does the emperor have no clothes?. *Abdom Radiol (NY)* 2017; 42: 342–345.
8. Sidhu HS, Benigno S, Ganeshan B, et al. “Textural analysis of multiparametric MRI detects transition zone prostate cancer”. *Eur Radiol* 2017; 27: 2348–2358.
9. Algohary A, Viswanath S, Shiradkar R, et al. Radiomic features on MRI enable risk categorization of prostate cancer patients on active surveillance: preliminary findings. *J Magn Reson Imaging* 2018. doi: 10.1002/jmri.25983.
10. Shiradkar R, Ghose S, Jambor I, et al. Radiomic features from pretreatment biparametric MRI predict prostate cancer biochemical recurrence: preliminary findings. *J Magn Reson Imaging* 2018; 48: 1626–1636.
11. Gnep K, Fargeas A, Gutiérrez-Carvajal RE, et al. Haralick textural features on T2-weighted MRI are associated with biochemical recurrence following radiotherapy for peripheral zone prostate cancer. *J Magn Reson Imaging* 2016; 45: 103–117.
12. Khoo CC, Miah S, Connor MJ, et al. A systematic review of salvage focal therapies for localised non-metastatic radiorecurrent prostate cancer. *Transl Androl Urol* 2020; 9: 1535–1545.
13. Byrne NM, Nesbitt H, Ming L, et al. Androgen deprivation in LNCaP prostate tumour xenografts induces vascular changes and hypoxic stress, resulting in promotion of epithelial-to-mesenchymal transition. *Br J Cancer* 2016; 114: 659–668.
14. Montironi R, Cheng L, Scarpelli M, et al. Pathology and genetics: tumours of the urinary system and male genital system: clinical implications of the 4th Edition of the WHO classification and beyond. *Eur Urol* 2016; 70: 120–123.
15. Tixier F, Um H, Young RJ, et al. Reliability of tumor segmentation in

- glioblastoma: impact on the robustness of MRI-radiomic features. *Med Phys* 2019; 46: 3582–3591.
16. Duron L, Balvay D, Vande Perre S, et al. Gray-level discretization impacts reproducible MRI radiomics texture features. *PLoS One* 2019; 14: e0213459.
 17. Christie DR, Sharpley CF, Mitina N, et al. Is prospective MRI mapping of the changes in the volume of the prostate gland in prostate cancer patients undergoing 6 months of neo-adjuvant androgen deprivation therapy a step towards a trial to determine those who may benefit from treatment intensification or extended duration?. *J Med Imaging Radiat Oncol* 2020; 64: 287–292.
 18. Groenendaal G, Vulpen MV, Pereboom SR, et al. The effect of hormonal treatment on conspicuity of prostate cancer: implications for focal boosting radiotherapy. *Radiother Oncol* 2012; 103: 233–238.
 19. Van Son MJ, Peters M, Moerland MA, et al. MRI-guided ultrafocal salvage high-dose-rate brachytherapy for localized radiorecurrent prostate cancer: updated results of 50 patients. *Int J Radiat Oncol Biol Phys* 2020; 107: 126–135.
 20. Daniel M, Kuess P, Andrzejewski P, et al. Impact of androgen deprivation therapy on apparent diffusion coefficient and T2W MRI for histogram and texture analysis with respect to focal radiotherapy of prostate cancer. *Strahlenther Onkol* 2019; 195: 402–411.
 21. Lin YC and Huang HM. Denoising of multi b-value diffusion-weighted MR images using deep image prior. *Phys Med Biol* 2020; 65: 105003.
 22. Chen YL, Lin YJ, Lin SH, et al. The effect of spatial resolution on the reproducibility of diffusion imaging when controlled signal to noise ratio. *Biomed J* 2019; 42: 268–276.